6564 *Chem. Mater.* **2010,** *22,* 6564–6574
DOI:10.1021/cm102158w

CHEMISTRY OF MATERIALS
Article

Hydrothermal Synthesis and Surface Characteristics of Novel Alpha Alumina Nanosheets with Controlled Chemical Composition

Wojciech L. Suchanek,*[,†] Juan M. Garcés,[‡] Pasquale F. Fulvio,[§,⊥] and Mietek Jaroniec[§]

[†]*Sawyer Technical Materials, LLC, 35400 Lakeland Boulevard, Eastlake, Ohio 44095, United States,* [‡]*Consultant, LLC, 1106 West Sugnet Road, Midland, Michigan 48640, United States, and* [§]*Department of Chemistry, Kent State University, Williams Hall, Kent, Ohio 44242, United States.* [⊥]*Present address: Oak Ridge National Laboratory, Chemical Sciences Division, Oak Ridge, TN 37831, United States.*

Received July 31, 2010. Revised Manuscript Received November 8, 2010

Novel alpha alumina (α-Al_2O_3) nanosheets with controlled chemical compositions were synthesized at 450 °C under 10.3 MPa pressure by the hydrothermal treatment of boehmite powder (γ-AlOOH) in the presence of soluble salts of metal dopants, α-Al_2O_3 seeds, and 5% SiO_2 morphology modifier. Detailed XRD, SEM, HRTEM, STEM, and XEDS characterization was performed and it was found that the as-synthesized nanosheets were in most cases the phase-pure α-Al_2O_3 crystals exhibiting very strong (001) faceting, thicknesses of 10−50 nm, aspect ratios up to a few hundreds, and specific surface areas up to 35 m^2/g. Metal dopants from nearly every group of the Periodic Table were present in these α-Al_2O_3 nanosheets in concentrations up to ~0.5 atom % either as solid solutions or as nanosized inclusions. A thorough surface analyses using X-ray photoelectron spectroscopy (XPS), measurements of nitrogen adsorption isotherms at −196 °C, temperature-programmed desorption (TPD), and zeta potential measurements, revealed a very wide range of control of the surface charge, surface purity, and acid−base properties of the α-Al_2O_3 nanosheets by selection of different dopants and controlling their distribution within the nanosheets. The BET surface area values of the hydrothermally synthesized nanosheets were stable up to 1200 °C. Such novel doped α-Al_2O_3 nanomaterials can be useful in a variety of applications such as catalysis, chemical-mechanical planarization, composites, and ceramics.

Introduction

Nanosized alpha alumina (α-Al_2O_3, corundum) is attractive for a multitude of applications due to favorable combination of such properties as high mechanical strength and hardness, good wear resistance, low electric conductivity, high refractoriness, and corrosion resistance.[1] In catalysis, nanosized α-Al_2O_3 powders are being sought as thermally stable alternative to widely used transition aluminas, which undergo phase transformations during their high-temperature use, which is associated with significant surface area loss.[2] Similar problem of thermal instability occurs in alumina filtration membranes, which could be solved by employing stable nanosized α-Al_2O_3 powders to make them.[3] Another use of nanosized α-Al_2O_3 is in abrasive applications, including chemical-mechanical planarization (CMP), where small abrasive particles with uniform size distributions and controlled morphologies can be successfully used. Nanosized particles of hard corundum phase can be incorporated in polymer composites, also in paints, varnishes, coatings, etc., in order to enhance their mechanical properties. In addition, high-strength dense α-Al_2O_3 ceramics can be prepared from nanosized α-Al_2O_3 powders at reduced temperatures.[3,4]

Nanosized α-Al_2O_3 powders can be synthesized by several high-temperature methods, such as calcination of precursor gels at 800−1000 °C,[4−6] pyrolysis of complex compounds above 1000 °C,[7] emulsion processing followed by calcination above 1000 °C.[8] One of the low-temperature methods involves calcination of diaspore (α-AlOOH) at 500 °C,[9] with limited morphology control of nanosized α-Al_2O_3 powders, which are formed as pseudomorphs of diaspore.[10] Another low-temperature approach to nanosized α-Al_2O_3 is calcination of gels also at about 500 °C.[9] That approach involves the use of toxic alkoxides, thus is expensive and not environmentally

*Corresponding author. E-mail: wls@SawyerLLC.com or w_suchanek@yahoo.com. Tel: 440-951-8770, ext. 265. Fax: 440-951-1480.

(1) Richards, G. In *Encyclopedia of Materials Science and Engineering*; Bever, M. B., Ed.; Pergamon Press/The MIT Press: Cambridge, MA, 1986; Vol. *1*, pp 158−162.
(2) Horiuchi, T.; Sugiyama, T.; Mori, T. *J. Mater.Chem.* **1993**, *3*, 861.
(3) Ma, H.; Krell, A.; Buse, F. *Chem. Eng. Technol.* **2001**, *24*, 1005.
(4) Li, J. G.; Sun, X. *Acta Mater.* **2000**, *48*, 3103.
(5) Krell, A.; Ma, H. *J. Am. Ceram. Soc.* **2003**, *86*, 241.
(6) Zhang, X.; Ge, Y.; Hannula, S.-P.; Levänen, E.; Mäntylä, T. *J. Mater. Chem.* **2005**, *18*, 2423.
(7) Pati, R. K.; Ray, J. C.; Pramanik, P. *J. Am. Ceram. Soc.* **2001**, *84*, 2849.
(8) Lin, C.-P.; Wen, S.-B.; Lee, T.-T. *J. Am. Ceram. Soc.* **2002**, *85*, 129.
(9) Perotta, A. J. *Mater. Res. Innovat.* **1998**, *2*, 33.
(10) Mönch, B.; Werner, G.; Tomandl, G. In *Proceedings of the 9th CIMTEC− World Ceramic Congress* (*Ceramics: Getting into the 2000's−Part B*); Vincenzini, P., Ed.; Techna Srl: Biella, Italy, 1999; pp 11−18.

Published on Web 12/06/2010

friendly. All these methods typically produced nanosized α-Al_2O_3 powders with equiaxed morphology and high level of aggregation.

However, in all applications discussed above, a precise control of the morphology and chemical composition of the nanosized α-Al_2O_3 powders is of great importance. Morphology of the nanoparticles can have tremendous impact on catalytic selectivity,[11,12] microstructure, and mechanical performance of materials.[13−15] In addition, chemical dopants can provide active centers for catalysis, modify acid/base properties of the catalytic supports, change the surface energy, or electric charge. Such modifications may be essential in catalytic applications, dispersibility of the nanomaterials, interactions with polymers, etc. In high-temperature applications, the chemical dopants can also modify thermal stability and/or sinterability of the α-Al_2O_3 powders, enhancing or constringing densification, grain growth, etc.

Recently, Suchanek and Garcés synthesized novel α-Al_2O_3 nanosheets (ANS) by the hydrothermal technique.[16,17] Hydrothermal synthesis is an environmentally benign technology, which can crystallize materials directly from aqueous media at low temperatures under moderate to high pressures.[18−21] So far, only a few works have been devoted to the low-temperature (~400 °C) hydrothermal synthesis of α-Al_2O_3 with limited emphasis on morphology control, particularly in the nanosize range.[22] In the present work, we explore for the first time a hydrothermal method to synthesize thermally stable α-Al_2O_3 nanosheets with a wide range of metal dopants from nearly every group of the Periodic Table. The dopants in concentrations up to about 0.5 at % were either incorporated in the α-Al_2O_3 lattice or formed nanosized inclusions. In most cases, doping did not significantly change morphology or BET surface areas of the nanosheets but modified their chemical composition by introducing active sites on the surface, as confirmed by a thorough surface analysis.

Experimental Section

Materials. The hydrothermal synthesis of about 200 g of undoped α-Al_2O_3 nanosheets (reference) was performed as follows. A 1 L titanium container was thoroughly cleaned and 287 g of deionized water was added to it. Then, 1.06 g of 96.6% H_2SO_4 was added to the container and its content was stirred. Subsequently, 231 g of commercial boehmite powder was added to the container and stirred to obtain uniform slurry. The boehmite powder had BET surface area of 180 m^2/g, median particle size of 25 μm, and low impurities content (150 ppm Na, 55 ppm Fe, 75 ppm Si). Then, 23.1 g (i.e., 10 wt % with respect to the boehmite weight) of commercial nanosized α-Al_2O_3 seeds, with agglomerate size of 1 μm, were added to the container and the slurry was vigorously stirred again for about 3 min. Finally, 28.9 g of nanosized colloidal silica aqueous dispersion (40% SiO_2, AS-40, Ludox) as morphology modifier in concentration of 5 wt % with respect to the boehmite was added to the container and its content was stirred again for 3 min.

The hydrothermal synthesis of about 200 g of doped α-Al_2O_3 nanosheets were performed using a similar method. One-liter titanium containers were thoroughly cleaned and 387 g of deionized water was added to each of them. The amount of water was determined experimentally to allow good flow of the precursor slurries during mixing. Then, 1.06 g of 96.6% H_2SO_4 was added to each container and their contents were stirred. Subsequently, 0.69 or 6.93 g of chemical additives, i.e., 0.3 or 3.0 wt % with respect to the weight of boehmite, were added in order to introduce the doping elements (dopants) to the precursor slurries. The chemical additives were mostly in form of soluble salts of the doping elements, all reagent or ACS grades (Alfa Aesar, Ward Hill, MA or Spectrum Chemical, New Brunswick, NJ). $YCl_3 \cdot xH_2O$ was used to dope Y into α-Al_2O_3 nanosheets, $ZrOCl_2 \cdot 8H_2O$ was used for Zr, $ZnCl_2$ for Zn, $CuSO_4 \cdot 5H_2O$ for Cu, 20% $CoCl_2$ (aq) for Co, $NiCl_2$ for Ni, $CrCl_3 \cdot 6H_2O$ for Cr, $FeCl_3 \cdot 6H_2O$ for Fe, $SnCl_2$ for Sn, 20% $Ti_2(SO_4)_3$ (aq) for Ti, $NbCl_5$ for Nb, V_2O_5 for V, $CeCl_3 \cdot 5H_2O$ for Ce, $KMnO_4$ for Mn, $SbCl_3$ for Sb, $MoCl_5$ for Mo, $MgCl_2 \cdot 6H_2O$ for Mg, LiOH for Li, 50% CsOH (aq) for Cs, KCl for K, and $CaCl_2 \cdot 2H_2O$ for Ca. After complete dissolution or dispersion of the chemical additives upon stirring, 231 g of boehmite powder was added to the containers and stirred to obtain uniform slurry. Then, 23.1 g (i.e., 10 wt % with respect to the boehmite weight) of commercial nanosized α-Al_2O_3 seeds, with agglomerate size of 1 μm, were added to the container and the slurry was vigorously stirred again for about 3 min. Finally, 28.9 g of nanosized colloidal silica aqueous dispersion (40% SiO_2, AS-40, Ludox) as morphology modifier in concentration of 5% with respect to the boehmite was added to the container and its content was stirred again for 3 min.

The containers with the precursor slurries were placed into cleaned autoclave (264 L volume, custom-made, Autoclave Engineers, Erie, PA). Some deionized water was placed in the bottom of the autoclave. The autoclave was then sealed using modified Bridgman-type plug and covered with insulation. A calibrated pressure gauge and two J-type thermocouples were attached. The autoclave was heated from room temperature to 450 °C with a heating rate of 9.0 °C/h, followed by holding at the peak temperature for 10 days, with pressure about 10.3 MPa, controlled by pressure relief valve. Such synthesis conditions are dictated by the $Al_2O_3-H_2O$ phase diagram,[22] which shows the formation of the α-Al_2O_3 phase below 15 MPa, and thus requires pressure relief in order to avoid formation of the diaspore (α-AlOOH) phase. All water from the autoclave was vented after completing the heating cycle, at the temperature of about 400 °C. The as-synthesized materials were unloaded from the containers, ground, and subjected to a thorough characterization by XRD, SAXS, SEM, HRTEM, STEM, XEDS, measurements of nitrogen adsorption isotherms at −196 °C, XPS, and

(11) Freund, H.-J.; Libuda, J.; Bäumer, M.; Risse, T.; Carlsson, A. *Chem. Rec.* **2003**, *3*, 181.
(12) Lee, I.; Delbecq, F.; Morales, R.; Albiter, M. A.; Zaera, F. *Nat. Mater.* **2009**, *8*, 132.
(13) Clegg, W. J.; Kendall, K.; Alford, N. M.; Button, T. W.; Birchall, J. D. *Nature* **1990**, *347*, 455.
(14) Rühle, M.; Evans, A. G. *Prog. Mater. Sci.* **1989**, *33*, 85.
(15) Bonderer, L. J.; Studart, A. R.; Gauckler, L. J. *Science* **2008**, *319*, 1069.
(16) Suchanek, W. L.; Garcés, J. U.S. 2010/0159226 A1; Sawyer Technical Materials: Eastlake, OH, 2009.
(17) Suchanek, W. L.; Garcés, J. M. *CrystEngComm* **2010**, *12*, 2996.
(18) Suchanek, W. L.; Lencka, M. M.; Riman, R. E. In *Aqueous Systems at Elevated Temperatures and Pressures: Physical Chemistry in Water, Steam, and Hydrothermal Solutions*; Palmer, D. A., Fernández-Prini, R., Harvey, A. H., Eds.; Elsevier Ltd.: Amsterdam, 2004; pp 717−744.
(19) Riman, R. E.; Suchanek, W. L.; Lencka, M. M. *Ann. Chim. Sci. Mat.* **2002**, *27*, 15.
(20) Byrappa, K.; Yoshimura, M. *Handbook of Hydrothermal Technology*; Noyes Publications/William Andrew Publishing LLC: Norwich, NY, 2001.
(21) Byrappa, K.; Adschiri, T. *Prog. Cryst. Growth Charact. Mater.* **2007**, *53*, 117.
(22) Suchanek, W. L. *J. Am. Ceram. Soc.* **2010**, *93*, 399.

TPD (see definitions and detailed descriptions in the Characterization Methods section).

However, to investigate the thermal stability of the doped and undoped α-Al_2O_3 nanosheets, as-synthesized materials were heat-treated in air at temperatures between 1000 and 1200 °C for 12−24 h in a furnace with $MoSi_2$ heating elements (Carbolite, model RHF17/25, Watertown, WI). The heating rate was 2.0 °C/min in all cases. The furnace was cooled to the room temperature in an uncontrolled fashion. The heat-treated α-Al_2O_3 nanosheets were characterized by measurements of nitrogen adsorption isotherms at −196 °C only.

Several equiaxed α-Al_2O_3 powders were used as references, and thus compared with the α-Al_2O_3 nanosheets in such surface analyses as measurements of nitrogen adsorption isotherms at −196 °C, TPD and Zeta potential measurements (see detailed descriptions in the Characterization Methods section). The reference powders were: (i) AKP-50 (Sumitomo Materials, Tokyo, Japan) with primary particle size of 100−300 nm, BET specific surface area of 12 m^2/g, and >99.99% chemical purity (4 ppm Na, 5 ppm Fe, 15 ppm Si); (ii) hydrothermally synthesized AO-128 (Sawyer Technical Materials, LLC, Eastlake, OH) with BET specific surface area of 9.4 m^2/g, primary particle size of ∼250 nm, and 99.9% chemical purity (500 ppm Na, 110 ppm Fe, 30 ppm Si); and (iii) hydrothermally synthesized AO-236 (Sawyer Technical Materials, LLC, Eastlake, OH) with BET specific surface area of 9.7 m^2/g, primary particle size of ∼100 nm, and 99.85% chemical purity (120 ppm Na, 20 ppm Fe, 170 ppm Si). All reference powders were thoroughly analyzed by XRD, SEM, and XPS (see detailed description in the next section).

The undoped α-Al_2O_3 nanosheets are denoted as ANS. All metal (Me) doped α-Al_2O_3 nanosheets (ANS) are denoted as Me-ANS, for instance Ni-ANS denotes Ni-doped α-Al_2O_3 nanosheets. The equiaxed α-Al_2O_3 reference powders are denoted using their commercial names, i.e., as AKP-50, AO-236, and AO-128.

Characterization Methods. Phase composition of all as-synthesized and reference materials was characterized by X-ray diffraction (XRD) on an Advanced Diffraction System X1 diffractometer (Scintag Inc., Cupertino, CA) using Cu K_α radiation, in the 2Θ range between 10 and 70° with a 0.05° step size and 0.3−1.0 s count time. The identification of the materials was determined by comparing the experimental XRD patterns to JCPDS standards, i.e., card 10−0173 for α-Al_2O_3 (corundum) and 03−0066 for γ-AlOOH (boehmite).

Selected as-synthesized materials were analyzed by small-angle X-ray scattering (SAXS) technique; the SAXS patterns were recorded on a Bruker Nanostar-U instrument (Bruker AXS Inc., Madison, WI) equipped with Cu K_α radiation source (λ = 1.54184 Å), which was a rotating anode operated at 50 kV and 24 mA, in the 2Θ range of 0.1−3.0° with 0.005° step size.

The morphology and phase purity of the as-synthesized and reference α-Al_2O_3 nanomaterials were examined using scanning electron microscope (SEM, model S-4500, Hitachi, Japan) at 5 kV accelerating voltage. Prior to the SEM examination, the materials were attached to aluminum holders using conductive carbon tape and subsequently sputtered with thin conductive layers of palladium or gold.

Chemical compositions of all as-synthesized α-Al_2O_3 nanosheets were determined using either DC arc emission spectroscopy (DC Arc), inductively coupled plasma (ICP), or Inductively Coupled Plasma-Mass Spectroscopy (ICP-MS) at NSL Analytical Services, Inc. (Cleveland, OH). Chemical moieties present on the external surfaces and in the 6−12 nm deep subsurface regions of the as-synthesized and reference α-Al_2O_3 materials were determined by X-ray photoelectron spectroscopy (XPS) using the Phi 5600 ESCA system (Physical Electronics, Inc., Chanhassen, MN). The materials were attached to the holders using conductive carbon tape. The XPS spectra were acquired from the surface spots with diameters of approximately 0.3 mm on each sample. At least one spot on each sample was analyzed by this technique. In a typical XPS measurement, a 20−60 min overview scans (0.4 eV step) and high-resolution scans (0.1 eV step) were performed in the binding energy range of 0−1100 eV (0−1400 eV in Mg-doped samples).

Transmission electron microscopy in high-resolution (HRTEM) and scanning (STEM) modes and X-ray energy-dispersive spectroscopy (XEDS) were performed on selected as-synthesized α-Al_2O_3 nanosheets using field-emission gun energy-filtering transmission electron microscope Libra 200FE (Carl Zeiss SMT Inc., Peabody, MA) with the acceleration voltage of 200 kV. Prior to the TEM examination, the α-Al_2O_3 powders were ultrasonically dispersed in isopropanol, transferred onto Cu grids, and subsequently dried under IR heat lamp.

Nitrogen gas adsorption isotherms measurements were performed at temperature of −196 °C on the reference, as-synthesized, and heat-treated materials using volumetric adsorption analyzers (models ASAP 2010 and 2020, Micromeritics, Norcross, GA). Before adsorption measurements the alumina samples were degassed under vacuum for at least 2 h at 200 °C. The specific surface area of the samples was calculated using the Brunauer−Emmett−Teller (BET) method within the relative pressure range of 0.05 to 0.20.[23]

Ammonia and carbon dioxide temperature-programmed desorption experiments, NH_3-TPD and CO_2-TPD, respectively, were performed on selected as-synthesized and reference α-Al_2O_3 materials using Auto Chem II Chemisorption Analyzer (Micromeritics, Norcross, GA) equipped with a thermocouple detector (TCD). Approximately 250 mg of each sample were loaded in a quartz tube micro reactor supported by quartz wool and degassed at 500 °C for 1 h before NH_3 and for 2 h before CO_2 using heating rate of 5 °C/min in flowing He (50 cm^3/min). Next, the samples were cooled to 120 °C and exposed to flowing 5% NH_3−He (50 cm^3/min) for 1 h or 5% CO_2−He and finally purged in flowing He for 1 h. For desorption, the samples were heated to 500 °C for 30 min (NH_3-TPD) or 750 °C for 60 min (CO_2-TPD) at 10 °C/min. The amounts of desorbed NH_3 and CO_2 were obtained by integration of the desorption profiles and referenced to the TCD signals calibrated for known volumes of analysis gases.

Zeta potential measurements were performed on selected as-synthesized and reference α-Al_2O_3 powders using Nanosizer ZS with autotitrator (Malvern Instruments Ltd., Worcestershire, UK). 0.25 M-NaOH and 0.25 M-HCl aqueous solutions were used for titration in the pH range of 2−12. Isoelectric points were determined from each measurement.

Results and Discussion

Properties of the Metal-Doped α-Al_2O_3 Nanosheets. Table 1 summarizes typical properties of the doped α-Al_2O_3 nanosheets (Me-ANS) synthesized by the hydrothermal method in the present work, such as the dopant concentrations, uniformity of the dopant distribution, phase compositions, BET surface areas, and thermal stabilities. For comparison, properties of undoped α-Al_2O_3 nanosheets (ANS), synthesized under similar conditions

(23) Kruk, M.; Jaroniec, M. *Chem. Mater.* **2001**, *13*, 3169.

Table 1. Properties of Selected Doped α-Al_2O_3 Nanosheets Synthesized by the Hydrothermal Method in the Present Work

sample	chemical additives in the precursor (conc in wt%)[c]	dopant concentration in as-synthesized materials as measured by different methods (at %)			uniformity of dopant concentration in as-synthesized materials		phase composition of the as-synthesized materials, by XRD	BET surface area (m^2/g)	
		XPS surface	XPS bulk	ICP/DC Arc bulk [d]	by XPS	by STEM		as-synthesized	heat-treated at 1200 °C for 24 h
ANS	0% (reference)						100% α-Al_2O_3	19.1	21.4[a]
Ti-ANS	3.0% $Ti_2(SO_4)_3$	0.32	0.35	0.37	uniform	uniform	α-Al_2O_3 + γ-AlOOH (<)	26.7	16.2
Zr-ANS	3.0% $ZrOCl_2$	0.38	0.41	0.20	uniform	10−20 nm inclusions	100% α-Al_2O_3	28.4	21.2
V-ANS	3.0% V_2O_5	0.41	0.36	0.73	uniform		α-Al_2O_3 + γ-AlOOH (<)	25.4	2.7
Nb-ANS	0.3% $NbCl_5$	0.02	0.01	0.03	uniform		100% α-Al_2O_3	23.2	20.2
Cr-ANS	3.0% $CrCl_3$	0.27	0.26	0.24	uniform	uniform	100% α-Al_2O_3	23.1	19.3
Mo-ANS	3.0% $MoCl_5$	0.33	0.37	0.25	uniform		100% α-Al_2O_3		
Mn-ANS	3.0% $KMnO_4$	0.26	0.22	0.41	uniform	uniform	100% α-Al_2O_3	23.0	3.8
Fe-ANS	3.0% $FeCl_3$	0.09	0.11	0.18	uniform	uniform	100% α-Al_2O_3	22.6	21.2
Co-ANS	3.0% $CoCl_2$	0.3	0.4[b]	0.37	uniform	uniform	α-Al_2O_3 + tr. impurities	10.9	9.7
Ni-ANS	3.0% $NiCl_2$	0.16	0.14	0.16	uniform	1−2 nm clusters	α-Al_2O_3 + tr. impurities	11.7	15.2
Cu-ANS	0.3% $CuSO_4$	0.03	0.02	0.02	uniform		100% α-Al_2O_3	22.3	15.7
Zn-ANS	3.0% $ZnCl_2$	0.08	0.04	0.001	surf. acc.[e]		α-Al_2O_3 + tr. impurities	14.5	12.5
Sn-ANS	0.3% $SnCl_2$	0.01	0.01	0.04	uniform	uniform	100% α-Al_2O_3	21.6	22.3
Sb-ANS	3.0% $SbCl_3$	0.4	0.1	0.19	surf. acc.[e]		100% α-Al_2O_3	35.9	21.9
Li-ANS	0.3% LiOH	N/D[f]	N/D[f]	0.12			100% α-Al_2O_3	19.7	13.6
K-ANS	3.0% KCl	0.40	0.22	0.75	surf. acc.[e]		α-Al_2O_3 + γ-AlOOH (tr.)	18.4	9.8
Cs-ANS	3.0% CsOH	N/D[f]	N/D[f]	0.44			100% α-Al_2O_3	21.9	20.6
Mg-ANS	3.0% $MgCl_2$	0.49	0.38	0.13	surf. acc.[e]	(uniform)	100% α-Al_2O_3	15.7	10.2
Ca-ANS	3.0% $CaCl_2$	0.08	0.07	0.19	uniform	10−20 nm inclusions	100% α-Al_2O_3	23.6	21.8
Ce-ANS	3.0% $CeCl_3$	0.04	0.06	0.06	uniform		α-Al_2O_3 + γ-AlOOH (<)	20.7	20.4

[a] Measured after heat treatment at 1000 °C for 12 h. [b] Measured by Auger electron spectroscopy (AES). [c] In some cases, hydrated forms of the salts listed were used. [d] Measurement error 10−15% of the reported value. [e] Surf. acc. denotes preferential accumulation of the metal dopant on the surfaces of the nanosheets. [f] N/D below detection limit of the XPS technique.

are also shown in Table 1. Dopants concentration ranged between 0.001 at % and 0.75 at %, and in most cases the dopants were uniformly distributed in the α-Al_2O_3 nanosheets. However, surface accumulation, inclusions, or clusters of dopants were also observed (Table 1).

Powder X-ray diffraction analysis (XRD) of the as-synthesized doped nanosheets revealed the presence of pure α-Al_2O_3 phase in most cases (Table 1, Figure 1). All as-synthesized powders exhibited very good crystallinity, as shown in Figure 1. However, composite powders with precursor-derived boehmite were also synthesized (Figure 1). The presence of unreacted γ-AlOOH (boehmite) in some samples was due to sluggish reaction kinetics, which was a function of the dopant type. It is in a good agreement with Al_2O_3−H_2O hydrothermal phase diagrams, which show that at temperatures above 380 °C and below 15 MPa pressure, boehmite converts directly into α-Al_2O_3 (corundum) phase without formation of any transition aluminas.[22] In a few cases, traces of not identified impurities were observed, quite likely oxides of the doping elements (Table 1). It was found in the previous work using HRTEM analysis and electron diffraction that the individual undoped α-Al_2O_3 nanosheets were single crystals with preferential c-faceting.[16,17] In the present work, high relative intensities of the XRD (300) peaks in all as-synthesized doped α-Al_2O_3 nanosheets, caused by texturing under pressure, are consistent with c-faceting of the individual crystallites (Figure 1). Full-width at half-maximum (fwhm) measurements of the XRD peaks revealed significant increase of the peak widths as compared to the equiaxed α-Al_2O_3 (AO-236), which could be associated with small size/thickness of the α-Al_2O_3 nanosheets and/or increasing lattice disorder. The exceptions here were only the (110) peaks, which remained narrow in all cases. This effect is again consistent with c-faceting of the doped α-Al_2O_3 nanosheets, which have widths in the order of hundreds nm in the ⟨110⟩ direction.

Small-angle X-ray scattering (SAXS) analysis was used to measure thickness of the undoped α-Al_2O_3 nanosheets (see Figure S1 in the Supporting Information). Only a single peak was observed in the 2Θ range of 0.1−3.0°. The peak was positioned at 0.17°, which corresponds to the spacing of 26 nm, and could be assigned to the thickness of the nanosheets in the absence of any other visible microstructural features. Absence of other SAXS peaks at higher angles indicates lack of periodic substructures within individual nanosheets. The measured thickness of 26 nm was in a good agreement with the thickness estimation from the SEM analysis for the undoped α-Al_2O_3 nanosheets. A comparison of the fwhm values of the (113) XRD peak in the undoped and doped α-Al_2O_3 nanosheets revealed fwhm variations of not more than ±20%, which corresponds to thickness variation of 21−31 nm, as calculated from the Scherrer equation.

SEM photographs shown in Figure 2b−f reveal typical morphologies of the as-synthesized doped α-Al_2O_3 nanosheets. Undoped α-Al_2O_3 nanosheets (ANS), synthesized under the same hydrothermal conditions, are also shown

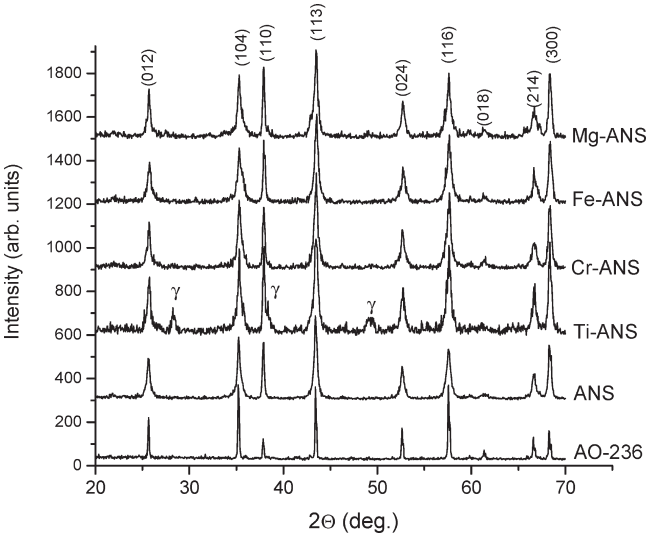

Figure 1. XRD patterns of the as-synthesized α-Al_2O_3 nanosheets prepared hydrothermally in the present work without dopants (ANS), and with such dopants as Ti (Ti-ANS), Cr (Cr-ANS), Fe (Fe-ANS), and Mg (Mg-ANS). For comparison, an equiaxed α-Al_2O_3 reference powder (AO-236) is shown. Each pattern shows pure-phase α-Al_2O_3 (corundum), except for the composition with Ti, which is a mixture of α-Al_2O_3 and γ-AlOOH (boehmite, peaks marked with γ).

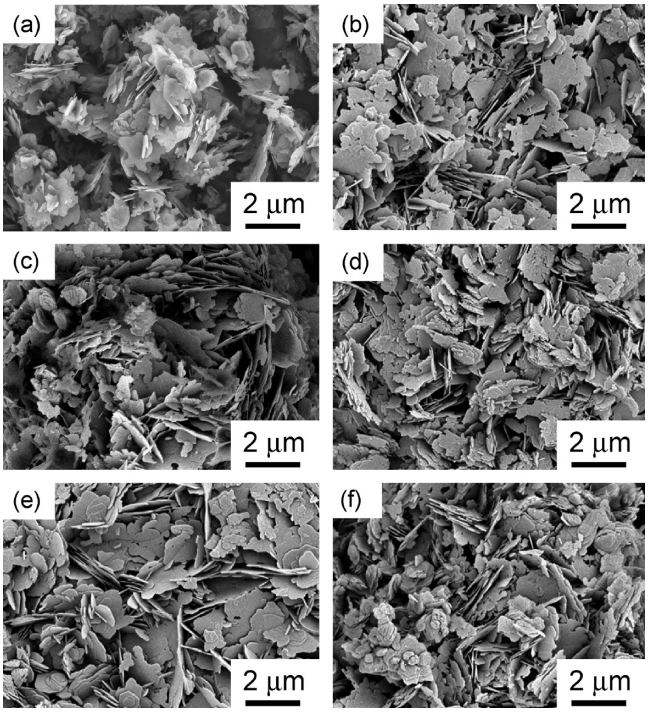

Figure 2. SEM photographs of the as-synthesized α-Al_2O_3 nanosheets, prepared hydrothermally (a) without dopants (ANS) and with such dopants as (b) Ni (Ni-ANS), (c) Co (Co-ANS), (d) Ti (Ti-ANS), (e) Li (Li-ANS), and (f) Ca (Ca-ANS). Magnifications are the same in all cases.

in Figure 2a for comparison. Aspect ratio of the doped α-Al_2O_3 nanosheets ranged between 10 and 200, their thicknesses were between 10 and 50 nm, and widths were between 0.5 and 3 μm (Figure 2). The thicknesses of the doped α-Al_2O_3 nanosheets estimated from the SEM agreed reasonably well with the results of the XRD/SAXS analyses, taking into consideration the thickness distribution of nanosheets in individual samples. Although some differences were apparent in samples with various dopants, individual crystallites of the doped α-Al_2O_3 nanosheets exhibited morphology and levels of aggregation comparable to the undoped α-Al_2O_3 nanosheets, regardless of the dopants used. The nanosheets formed large spherical aggregates with diameters in excess of 30 μm but some of them were relatively well dispersed. Within the aggregates and agglomerates, individual crystallites were either randomly connected or stacked together and connected by large facets (Figure 2).

In our previous work,[16,17] we found silica to be a very efficient morphology modifier for α-Al_2O_3. Silica tends to preferentially adsorb on the c-facets of the α-Al_2O_3 crystals, resulting in growth impediment along the *c*-axis, thus in the formation of platy morphologies, and in extreme cases, α-Al_2O_3 nanosheets.[16,17] Concentration of SiO_2 was optimized at the level of 5 wt % to produce doped and undoped α-Al_2O_3 nanosheets described in the present work. Bulk chemical analysis of the as-synthesized, undoped α-Al_2O_3 nanosheets, revealed the presence of 2.6 wt % of Si, which corresponds to 5.6 wt % of SiO_2. Surface concentration of Si, as measured by XPS, was 2.3 at % (3.4 wt %) in the undoped α-Al_2O_3 nanosheets and varied between 1.7 at % and 2.5 at %, i.e., 2.6−3.7 wt %, in the doped α-Al_2O_3 nanosheets (Table 2). Surface silica on the α-Al_2O_3 nanosheets would be expected to promote formation of acid and/or basic sites comparable to those found in alumino-silicates. The silica could be removed from the surface of the α-Al_2O_3 nanosheets by simple treatments in bases or acids as discussed elsewhere,[16,17] but some fraction of silica was retained in the α-Al_2O_3 lattice, which was revealed by XPS analysis.[17]

Thorough TEM analysis was performed to further investigate morphology of the nanosheets and to determine how uniformly were the dopants incorporated in the α-Al_2O_3 nanosheets. In most cases, the HRTEM pictures revealed multilayered nature of the nanosheets, which tend to stick together connected by their large c-facets (Figures 3a, 4a, and 5a). Individual well-dispersed nanosheets were too thin to detect small concentrations of dopants in their XEDS spectra. Therefore, large aggregates of nanosheets were used for this purpose (Figures 3d, 4d, S2-d, and S3-c). The XEDS analysis revealed the presence of small amounts of the doping elements in the nanosheets, and some exemplary XEDS spectra are shown in Figures 3c, 4c, S2-c, and S3-b. Subsequently, STEM analysis of the individual nanosheets was performed, which allows seeing contrast between elements with different atomic numbers (Z-contrast). If regions with high dopant concentration were present, such as dopant-rich inclusions or local accumulation of dopant in the nanosheet, STEM imaging would allow seeing them as regions with different (higher) brightness. In the case of Ti-ANS (Figure 3), Mn-ANS (Figure 4), Fe-ANS (see Figure S2 in the Supporting Information), and Cr-ANS (Figure S3 in the Supporting Information), HRTEM analysis revealed the absence of clearly visible inclusions, and STEM pictures showed no Z-contrast, which could be ascribed to dopant-related inhomogeneities or inclusions. Similar

Table 2. Surface Concentrations of Silicon and Isoelectric Points for Undoped and Selected Doped α-Al_2O_3 Nanosheets

experiment no.	morphology of particles	dopant type and surface concentration (at %)[a]	surface concentration of Si (at %)	pH for zeta potential of 0 mV (isoeletric point)
ANS	nanosheets	undoped	2.3	3.47
Ti-ANS	nanosheets	0.32% Ti-doped	1.7	5.96
Zr-ANS	nanosheets	0.38% Zr-doped	(2.4)	5.96
Nb-ANS	nanosheets	0.02% Nb-doped	2.2	4.97
Cr-ANS	nanosheets	0.27% Cr-doped	2.1	8.66
Mn-ANS	nanosheets	0.26% Mn-doped		3.59
Fe-ANS	nanosheets	0.09% Fe-doped	(2.1)	4.52
Co-ANS	nanosheets	0.3% Co-doped	2.5	
Ni-ANS	nanosheets	0.16% Ni-doped	2.3	
Cu-ANS	nanosheets	0.03% Cu-doped	2.1	
Cs-ANS	nanosheets	0.44% Cs-doped		3.28
Mg-ANS	nanosheets	0.49% Mg-doped	2.3	3.85
Ca-ANS	nanosheets	0.08% Ca-doped	1.7	6.38
AKP-50	equiaxed	undoped	0.0	8.19
AO-128	equiaxed	undoped	0.3	5.28
AO-236	equiaxed	undoped	0.9	6.86

[a] Surface concentrations of dopants measured by the XPS analysis.

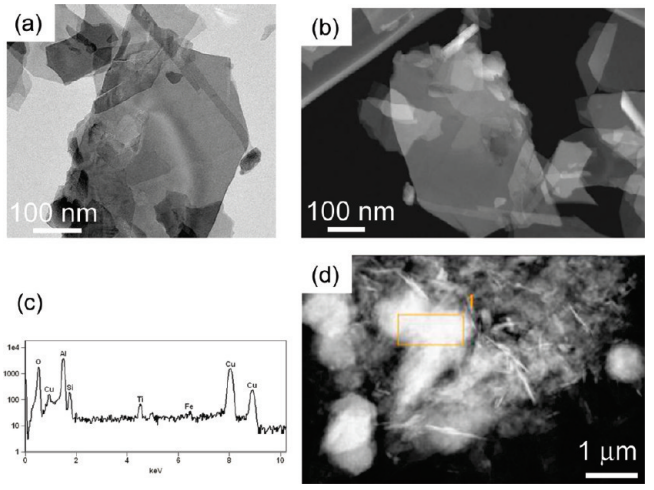

Figure 3. TEM analysis of hydrothermally synthesized Ti-doped α-Al_2O_3 nanosheets (Ti-ANS). (a) HRTEM image of the as-synthesized Ti-ANS revealing absence of any inclusions; several layers and broken pieces of the nanosheets are visible in addition to boehmite particles. (b) STEM images of the same nanosheets showing no Z-contrast, which confirms chemical uniformity of the dopants distribution in the material. (c) XEDS spectrum of an agglomerate (d) taken from the same sample clearly showing the presence of titanium (Ti) in addition to Al, O, Si (main constituents of the nanosheets), Cu, and C (constituents of the support grid); Fe peak is derived from the microscope hardware.

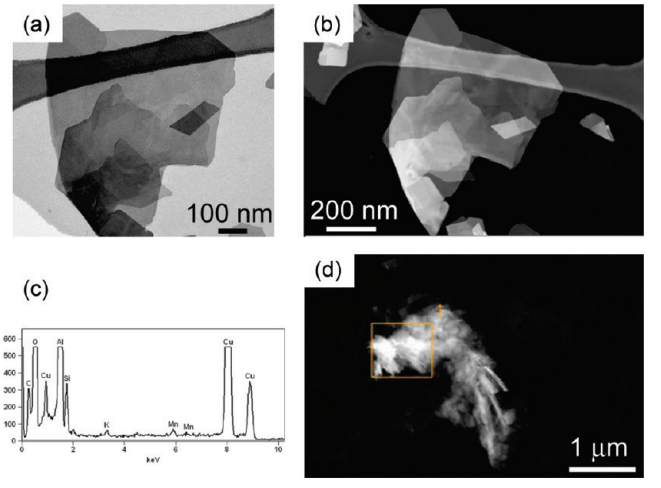

Figure 4. TEM analysis of hydrothermally synthesized Mn-doped α-Al_2O_3 nanosheets (Mn-ANS). (a) HRTEM image of the as-synthesized Mn-ANS revealing absence of any inclusions; several layers and broken pieces of the nanosheets are visible. (b) STEM images of the same nanosheets showing no Z-contrast, which confirms chemical uniformity of the dopants distribution in the material. (c) XEDS spectrum of an agglomerate (d) taken from the same sample clearly showing the presence of manganese (Mn) in addition to K (present in Mn salt used for doping), Al, O, Si (main constituents of the nanosheets), Cu, and C (constituents of the support grid).

HRTEM-STEM results were observed for Co-ANS and Mg-ANS (Figure S4a,b and Figure S5c,d in the Supporting Information). Such combination of HRTEM and STEM analysis is conclusive for Ti-, Mn-, Fe-, Cr-, and Co-doped nanosheets but confirms only the absence of inclusions in Mg-doped nanosheets. Because of the small contrast between Mg (Z = 12) and Al (Z = 13), the presence of inhomogeneities in dopant distribution cannot be precluded.

Interestingly, formation of inclusions was detected in Zr-doped nanosheets (Zr-ANS) both by HRTEM (Figure 5a) and TEM-XEDS (Figure 5b−d). The inclusions were 10−40 nm in diameter and they contained Zr-rich phase, possibly ZrO_2, quite uniformly distributed within the nanosheets. Inclusions of similar size in addition to dopant distribution inhomogeneities were also detected in the Ca-doped nanosheets (Ca-ANS), as shown in Figure S5 a-b (Supporting Information). In the case of Ni-ANS, small clusters (1−2 nm) of possibly Ni-rich phase were observed (Figure S4c,d in the Supporting Information). Thus, uniform doping in the lattice of the α-Al_2O_3 nanosheets can be accomplished with a variety of metals but in some cases it may result in the formation of dopant-rich particles or clusters. Such clusters or inclusions may be very useful in certain applications. In catalysis, presence of nanosized catalyst particles on an inert support is sometimes more desirable than homogeneous solid solutions. In composites, the formation of nanosized ZrO_2 particles within or on the α-Al_2O_3 nanosheets could act as an additional reinforcement of the material via transformation toughening mechanism.[14] Moreover,

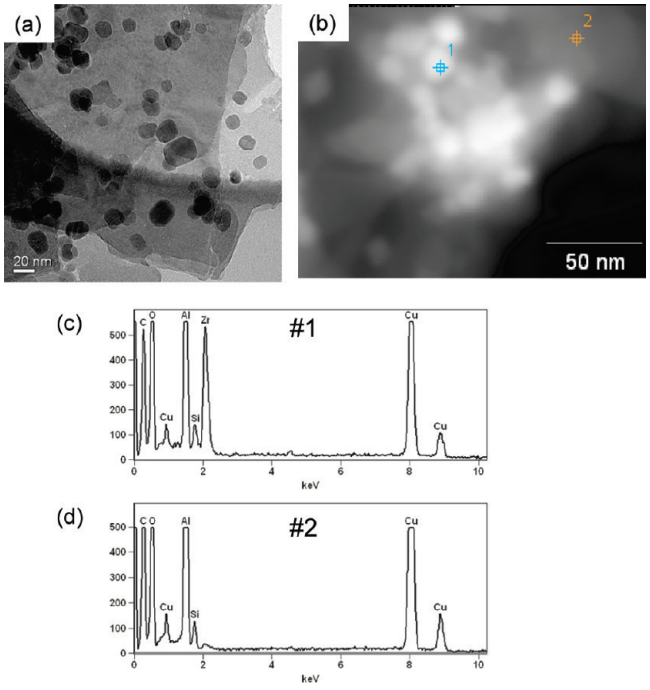

Figure 5. TEM analysis of hydrothermally synthesized Zr-doped α-Al_2O_3 nanosheets (Zr-ANS). (a) HRTEM image of the as-synthesized nanosheets revealing many inclusions, 10−40 nm in diameter; multilayered structure of the nanosheets is also visible. (b) TEM images of the same nanosheet showing significant Z-contrast, indicating different chemical composition of the inclusions and the nanosheets. (c) XEDS spectrum of an inclusion [point #1 in b] taken from the same sample clearly showing the presence of zirconium (Zr) in addition to Al, O, Si (main constituents of the nanosheets), Cu, and C (constituents of the support grid). (d) XEDS spectrum of a nanosheet region without inclusions [point #2 in b] taken from the same sample, which clearly shows low level or absence of Zr.

surface accumulation of small amounts of dopants can significantly modify a thin surface layer of the α-Al_2O_3 nanosheets and make it similar to the dopant-derived compounds while keeping the bulk properties of α-Al_2O_3 unchanged.

As summarized in Table 1, the BET specific surface areas of the doped α-Al_2O_3 nanosheets were at least 10 m^2/g and could be as high as 36 m^2/g, depending upon the type of dopant, For comparison, the BET surface area of the undoped nanosheets was ~20 m^2/g, thus the dopants did have an influence on the surface area of the doped nanosheets, which is determined primarily by their thickness and agglomeration. Certain reduction of the BET surface area was observed after heat treatment in air under extreme conditions, i.e., at 1,200 °C for 24 h, yet most nanosheets did not exhibit a significant BET surface area loss, particularly these doped with Fe, Co, Ni, Zn, Sn, Nb, Cr, Cs, Ca, Ce, and the undoped ones (Table 1). Such behavior of the doped α-Al_2O_3 nanosheets during heat treatment confirms generally their high thermal stability[16,17] and strong effect of certain dopants on acceleration of the diffusion processes, as manifested by their enhanced sinterability and surface area reduction. Among the materials studied, only Mn-ANS and V-ANS exhibited dramatic surface area loss at high temperatures.

We believe that the primary mechanism responsible for the thermal stability of the undoped and doped α-Al_2O_3 nanosheets is relatively small number of contacts between them, as compared to the equiaxed α-Al_2O_3 crystallites, which is due to the unique morphology of these nanoparticles. Various dopants and their combinations were investigated in sinterability studies of dense Al_2O_3 ceramics, thus it is difficult to make direct comparisons with the observed coarsening of some of the doped nanosheets. Nevertheless, TiO_2,[24,25] MnO_2,[26] $CuO+TiO_2$,[27] MnO_2-TiO_2,[25,26,28] MnO_2-SiO_2,[29] $CaO\text{-}ZnO\text{-}SiO_2$,[29] $CaO-SiO_2$,[28,30] $MgO-SiO_2$,[30] Y_2O_3+MgO,[31] $CuO+TiO_2+B_2O_3+MgO$,[32] or Fe_2O_3,[33] which were used as Al_2O_3 dopants or sintering additives, were found in various studies to enhance sintering kinetics and densification of Al_2O_3 ceramics. The α-Al_2O_3 nanosheets synthesized in the present work already contain SiO_2, which is used as a morphology modifier during their hydrothermal synthesis. Thus the surface area loss of the Mn-ANS, Ti-ANS, Cu-ANS, and Mg-ANS could be ascribed to the enhanced diffusion process and/or liquid phase formation caused by the dopants with or without SiO_2. On the contrary, Fe-ANS, Ca-ANS, or Zn-ANS nanosheets were quite thermally stable, confirming strong influence of the morphology on thermal stability.

Surface Characterization of the α-Al_2O_3 Nanosheets. *Nitrogen Adsorption Analysis.* Figure 6 shows nitrogen adsorption isotherms plotted in the form of relative adsorption vs relative pressure (in logarithmic scale) for selected metal-doped α-Al_2O_3 nanosheets in comparison to the undoped α-Al_2O_3 nanosheets (ANS) and the equiaxed α-Al_2O_3 reference powder (AKP-50). The relative adsorption is defined as the ratio of the volume of adsorbed nitrogen at a given relative pressure to the volume adsorbed corresponding to the BET monolayer capacity. Relative adsorption plots made in the submonolayer region are often used for comparison of the surface properties of solids because they account for differences in the surface area of the compared materials. A comparison of the relative adsorption plots displayed in Figure 6 shows a significant difference between α-Al_2O_3 nanosheets and equiaxed nanoparticles (AKP-50 powder). The aforementioned adsorption plots for undoped and doped α-Al_2O_3 nanosheets shown in Figure 6 feature a distinct step at the relative pressure of about 0.001 reflecting the formation of nitrogen monolayer on energetically homogeneous surface of these nanosheets.[34] The lack of big differences between relative adsorption curves for α-Al_2O_3

(24) Mishra, R. S.; Mukherjee, A. K.; Yamazaki, K.; Shoda, K. *J. Mater. Res.* **1996**, *11*, 1144.
(25) Erkalfa, H.; Misirli, Z.; Baykara, T. *J. Mater. Process. Technol.* **1996**, *62*, 108.
(26) Erkalfa, H.; Misirli, Z.; Baykara, T. *Ceram. Int.* **1995**, *21*, 345.
(27) Zhang, Q. I.; Yang, H.; Zou, J. L.; Sun, H. P. *J. Electroceram.* **2007**, *18*, 225.
(28) Huang, X. W.; Wang, S. W.; Zhao, S. K.; Huang, X. X. *Mater. Res. Bull.*. **2002**, *37*, 1709.
(29) Borsa, C. E.; Ferreira, H. S.; Kiminami, R. H. G. A. *J. Eur. Ceram. Soc.* **1999**, *19*, 615.
(30) Galusek, D.; Riley, F. L. *Philos. Mag., A* **2002**, *82*, 2041.
(31) Lee, H. W.; Sacks, M. D. *J. Am. Ceram. Soc.* **1990**, *73*, 1894.
(32) Xue, L. A.; Chen, I.-W. *J. Am. Ceram. Soc.* **1991**, *74*, 2011.
(33) Tartaj, P.; Tartaj, J. *Acta Mater.* **2002**, *50*, 5.
(34) Kruk, M.; Li, Z.; Jaroniec, M.; Betz, W. R. *Langmuir* **1999**, *15*, 1435.

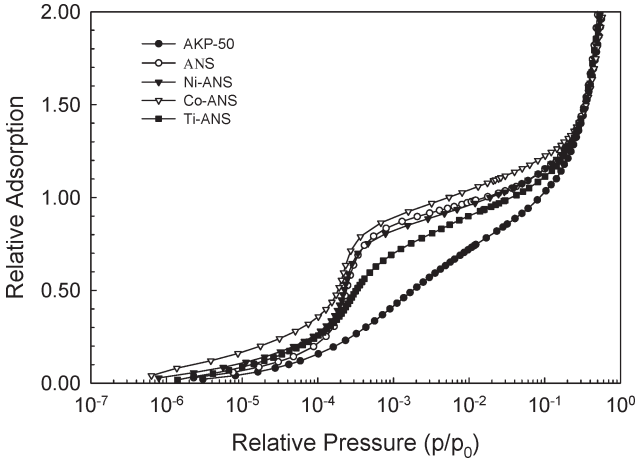

Figure 6. Relative nitrogen adsorption plotted as a function of relative pressure (in logarithmic scale) for undoped (ANS) and metal-doped (Ni-ANS, Co-ANS, and Ti-ANS) α-Al_2O_3 nanosheets in comparison to the equiaxed α-Al_2O_3 reference powder (AKP-50).

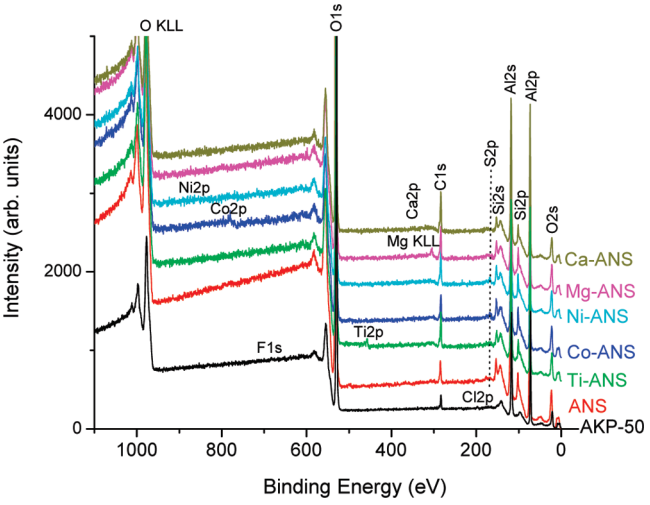

Figure 7. Overview XPS spectra of hydrothermally synthesized α-Al_2O_3 nanosheets, both doped and undoped. Sample numbers are marked. The spectra were acquired from the surfaces of the as-synthesized materials; no ion etching was applied in any case. For comparison, XPS spectrum of the surface of high-purity equiaxed α-Al_2O_3 powder (AKP-50) is shown. Except for the bands derived from Al, O, Si (main constituents of the nanosheets), C (CO_2 adsorption from the air), S derived from the hydrothermal crystallization environment, and weak lines from the doping elements, no impurities of any kind were observed. In the AKP-50 reference powder, Si, S, and dopants were absent, but traces of F and Cl on the surface were detected.

nanosheets with different metal dopants indicates that nitrogen molecule is not sensitive probe to detect changes upon metal doping. However, some changes are observed as in the case of Ti-doped α-Al_2O_3 nanosheets (Ti-ANS), which was probably because of the presence of boehmite particles. In contrast, the relative adsorption curve for the equiaxed α-Al_2O_3 reference powder (AKP-50) differs from those for undoped and doped α-Al_2O_3 nanosheets; the former shows a gradual increase with increasing relative pressure without distinct step reflecting monolayer formation. This behavior indicates much higher energetic heterogeneity of the equiaxed α-Al_2O_3 reference powder (AKP-50) in comparison to α-Al_2O_3 nanosheets.

XPS Analysis. XPS spectra acquired from the surfaces of the as-synthesized undoped and doped α-Al_2O_3 nanosheets are shown in Figure 7. The XPS analysis revealed that the chemical purity of the doped α-Al_2O_3 nanosheets was practically identical to the chemical purity of the undoped nanosheets, except for the content of dopants, which were intentionally added (Figures 7-8). The main constituents of all nanosheets were Al, O, and Si, but also C and S were detected (Figure 7). The presence of SiO_2-derived silicon on the surface of all as-synthesized nanosheets was caused by the use of 5 wt % SiO_2 morphology modifier in the synthesis. Carbon was most likely adsorbed from the air and the traces of sulfur were derived from H_2SO_4 used in the hydrothermal synthesis. Surprisingly, no chlorine-derived XPS peaks were detected in any case, although chlorides were typically used as soluble salts of the metal dopants (see Table 1). Doping modified the chemical composition of the α-Al_2O_3 nanosheets by introducing lattice defects, which could form active sites on their surface and in the bulk. The XPS analysis of the doped α-Al_2O_3 nanosheets revealed that almost in all cases dopants were present in the measured concentrations ranging from 0.01 to 0.4 at % (Table 1). Exceptions here were Li and Cs, which have low XPS sensitivity, and it is difficult to detect them at such low concentrations.

The XPS analysis was also used to determine presence of any differences of dopant concentrations between the surface and subsurface regions of the nanosheets (Table 1). In most cases, XPS revealed practically the same dopants concentrations both on the surface and in the bulk, at about 6−12 nm depths (Figure 8), which indicates lack of the surface accumulation of the dopants or dopants salts and is consistent with incorporation of the doping elements in the α-Al_2O_3 lattice. Some surface accumulation of dopants yet with high concentration in the bulk was observed in Sb-ANS, Zn-ANS, K-ANS, and Mg-ANS (Table 1). In the subsurface region, reduced silicon concentration was observed both in undoped and all doped α-Al_2O_3 nanosheets.

The XPS measurements were supplemented by the bulk chemical analysis of dopants concentrations in all as-synthesized samples. The results of the bulk chemical analysis were generally consistent with the bulk XPS analysis within the measurement error but some differences were apparent. The total dopant concentration in the nanosheets with surface concentration gradients was typically different from the bulk XPS data, which can be explained by sample inhomogenity (Zn-ANS, Sb-ANS, K-ANS, Mg-ANS). However, some differences were also observed for the samples with homogeneous dopant concentrations, such as Zr-ANS, V-ANS, Mn-ANS, Fe-ANS, Ca-ANS. In these cases, statistical measurement errors of the bulk ICP and DC Arc analyses ($\pm$10−15%) and the bulk XPS measurements (up to $\pm$50%) certainly contributed to such discrepancies. In addition, the well-known systematic errors of the bulk XPS measurements, such as differential sputtering, rough sample geometry, and surface effects could have contributed to a significantly larger analysis error, which is difficult to estimate quantitatively.

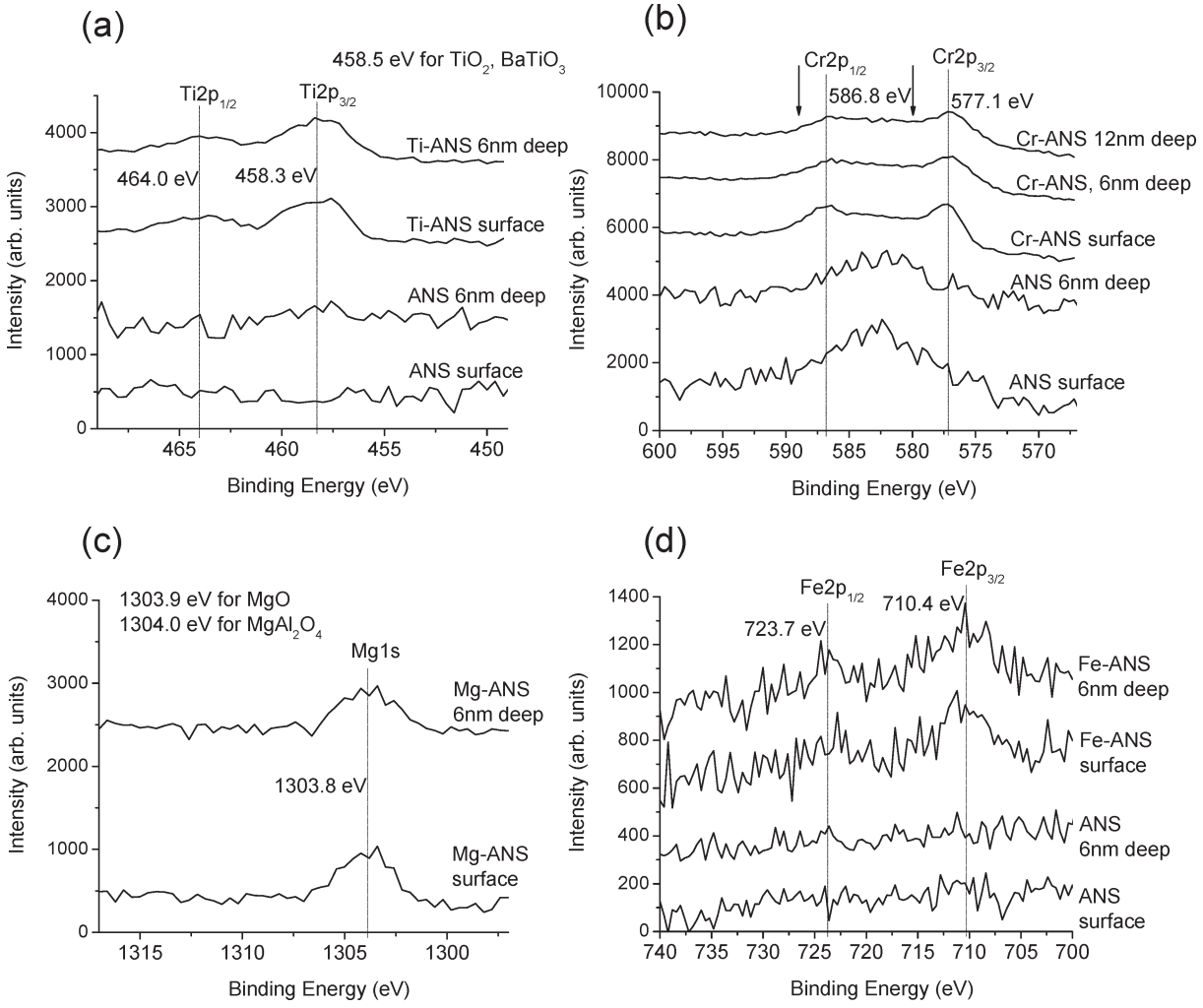

Figure 8. XPS spectra of hydrothermally synthesized α-Al_2O_3 nanosheets, undoped (ANS) and doped (a) Ti-ANS, (b) Cr-ANS, (c) Mg-ANS, and (d) Fe-ANS. The spectra were acquired both from the surfaces of the as-synthesized materials and from the subsurface regions 6−12 nm deep. Types and positions of all XPS bands are marked.

In most cases, the XPS and chemical analyses in conjunction with the TEM, SEM, and XRD data indicate the formation of doped α-Al_2O_3 nanomaterials, in which the dopants form chemically homogeneous solid solutions. Such chemical dopants could provide active centers for catalysis, modify acid/base properties of the catalytic supports, change the surface energy, or electric charge, and thus are important in many applications. To confirm this hypothesis, we performed zeta potential, NH_3-TPD, and CO_2-TPD measurements on selected α-Al_2O_3 nanosheets.

Zeta Potential. Relationship between zeta potential and solution pH was established for selected as-synthesized α-Al_2O_3 nanosheets and reference materials, which allowed calculations of the isoelectric points. The isoelectric point values for the nanosheets and reference materials are summarized in Table 2. The values of the isoelectric point were 3.5 for the undoped α-Al_2O_3 nanosheets and ranged between 3.3 and 8.7 for the doped α-Al_2O_3 nanosheets. These are not typical values for α-Al_2O_3 powders, which have isoelectric point generally at pH of 8−9.[35,36] However, the shift of the isoelectric point toward low pH can be explained by the presence of some SiO_2 on the surface, which alone has an isoelectric point at pH of 1−2.[37,38] High-purity reference α-Al_2O_3 powder (AKP-50) without any surface silica, but with traces of surface fluorine and chlorine (Figure 7), had the isoelectric point at pH of 8.2, whereas the other reference α-Al_2O_3 powders containing certain amounts of silica (AO-236 and AO-128) had this value at lower pH range from 5.3 to 6.9. Similar effect was reported in the literature during dispersing alumina powders in silica sol.[39] Unfortunately, no clear correlation between concentration of the surface silica ([Si] in at % as measured by XPS) and the isoelectric point pH could be established in the present work probably because of an overlapping effect with the dopants. For example, Cr-ANS has isoelectric point at pH 8.66, despite the presence of 2.1 at % Si on the surface, which points out toward strong influence of

(35) Johnson, S. B.; Scales, P. J.; Healy, T. W. *Langmuir* **1999**, *15*, 2836.
(36) Mikkola, P.; Ylha, P.; Levanen, E.; Rosenholm, J. B. *Ceram. Int.* **2004**, *30*, 291.
(37) Wen, X.-F.; Li, M.-Z.; Pi, P.-H.; Chen, J.; Yang, Z.-R. *Colloids Surf., A* **2008**, *327*, 103.
(38) Xu, G.; Zhang, J.; Song, G. *Powder Technol.* **2003**, *134*, 218.
(39) Zhu, X.; Jiang, D.; Tan, S.; Zhang, Z. *J. Eur. Ceram. Soc.* **2001**, *21*, 2879.

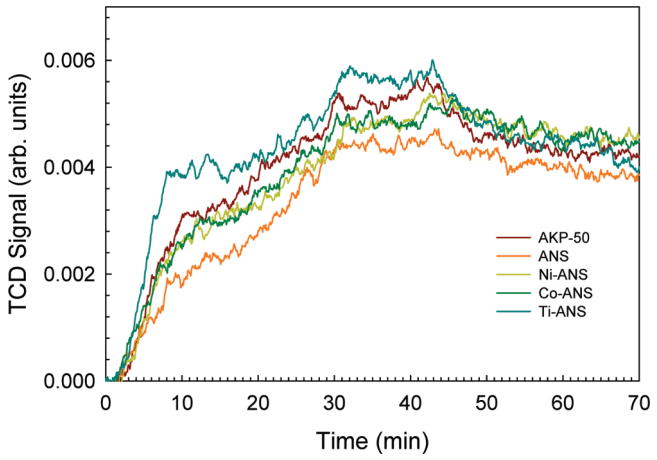

Figure 9. NH_3-TPD profiles for the doped (Co-ANS, Ni-ANS, and Ti-ANS) and undoped (ANS) α-Al_2O_3 nanosheets in comparison to the equiaxed α-Al_2O_3 reference powder (AKP-50). The area under the curves is proportional to the number of surface acid sites, whereas the temperature of desorption depends on the strength of these acid sites.

dopants on surface properties of the α-Al_2O_3 nanosheets. It is worth mentioning that zeta potential data for c-facets of α-Al_2O_3 single crystals were reported in several works, with isoelectric points scattered at pH between 4 and 7.[40−42] Therefore, it is possible that the preferential c-faceting of the α-Al_2O_3 nanosheets had certain contribution to lowering pH of the isoelectric point, in addition to the effects of the surface silica. Nevertheless, in the absence of other surface impurities (Figure 7), a wide range of isoelectrectric point pH from 3.3 through 8.7 indicates a pronounced effect of the dopants on the surface electric charge of the synthesized α-Al_2O_3 nanosheets. This feature could be utilized in ceramic processing of aluminas from the α-Al_2O_3 nanosheets, their dispersibility, interactions with other materials, composite processing, etc.

TPD Analysis. NH_3-TPD profiles for reference α-Al_2O_3 powders and selected as-synthesized undoped and metal-doped α-Al_2O_3 nanosheets are shown in Figure 9 and calculated parameters are summarized in Table 3. All materials exhibit similar desorption profiles with maximum desorption temperatures in the range of 380 to 400 °C. The total amounts of ammonia desorbed were calculated by integration of these profiles within the same desorption time frames. The undoped α-Al_2O_3 nanosheets and Ni-doped α-Al_2O_3 nanosheets (Ni-ANS) exhibited the lowest numbers of acid sites (~89 μmol/g) compared to the reference equiaxed α-Al_2O_3 (AKP-50) and the Co-ANS and Ti-ANS (> 110 μmol/g). It is interesting to note that, despite of similar number of sites as in the undoped α-Al_2O_3 nanosheets, the Ni-doped material has higher concentration of active sites (CAS) because of its lower specific surface area. As for Ti-ANS, despite of its considerably larger number of acid sites (127 μmol/g), its CAS was comparable to that of undoped α-Al_2O_3 nanosheets (ANS). In the case of Co-ANS having specific surface areas as low as half of that of undoped α-Al_2O_3 nanosheets, not only was the number of acid sites 26% higher than for pure alumina but the CAS was also approximately twice of that compared to the same reference.

Table 3. NH_3-TPD Data for Acid Sites for Undoped and Selected Doped α-Al_2O_3 Nanosheets

sample	S_{BET} (m^2 g^{-1})[a]	T_{max} (°C)[b]	V_{NH3} (cm^3STP g^{-1})[c]	n_{NH3} (μmol g^{-1})[d]	CAS (NH_3 nm^{-2})[e]
AKP-50	12.0	382	2.51	112	5.6
ANS	19.1	379	1.97	88	2.8
Ni-ANS	11.7	391	2.00	89	4.6
Co-ANS	10.9	378	2.48	111	6.1
Ti-ANS	26.7	396	2.85	127	2.9

[a] Specific surface area calculated in the relative pressure range of 0.05−0.20 using the BET equation. [b] Temperature of maximum rate of desorption. [c] Standard total volume of ammonia desorbed. [d] Amount of acid sites calculated by integration of the TPD profiles. [e] Surface concentration of active sites obtained from the amount of acid sites per unit area of the sample.

As for the CO_2-TPD experiments (Table 4), the samples of undoped α-Al_2O_3 nanosheets (ANS) and Mg-doped α-Al_2O_3 nanosheets (Mg-ANS) exhibited the highest numbers of basic sites, compared to the Li- and Ca-doped nanosheets (Li-ANS and Ca-ANS). In Figure S6 (Supporting Information), the TPD profiles of undoped α-Al_2O_3 and Mg-doped α-Al_2O_3 nanosheets show a strong desorption peak centered at approximately 670 °C. While Ca-doped α-Al_2O_3 nanosheets exhibited a small desorption peak at similar temperature, the Li-doped nanosheets may exhibit slightly weaker basic sites based on its lowest desorption temperature (626 °C). Also similar to the doping effects found for the acidic sites in other types of doped-aluminas, the Mg-doped α-Al_2O_3 nanosheets exhibit the CAS 30% higher than the undoped α-Al_2O_3 nanosheets, because of having smaller specific surface area (~16 m^2/g), see Table 4. The larger amounts of carbonate species formed on the basic surface sites of Mg-doped α-Al_2O_3 nanosheets when compared to Li- and Ca-doped ones may be the result of the highest Mg loading (see Table 1). The single and relatively narrow CO_2 desorption peak for Mg-doped α-Al_2O_3 nanosheets further reveal similar types and strength of basic sites to those of α-Al_2O_3 nanosheets despite of the gradient distribution of Mg within the oxide sheets. As for the Li-doped analogue having similar surface area to the undoped α-Al_2O_3 nanosheets and Li concentrations below the detection limit of XPS, its CAS was ~35% smaller than that of undoped α-Al_2O_3 nanosheets (9.4 CO_2/nm^2).

The results of the NH_3-TPD and CO_2-TPD analyses and zeta potential measurements clearly show that the surface properties of the α-Al_2O_3 nanosheets can be tailored in a wide range without changing bulk properties of these materials. Depending upon type of the metal dopant, the surface charge of the α-Al_2O_3 nanosheets can be changed from positive to negative and the nanosheets surfaces can be made acidic or basic. Thus, a variety of catalytic reactions could benefit from the use of the doped α-Al_2O_3 nanosheets-based catalysts or supports.

(40) Kershner, R. J.; Bullard, J. W.; Cima, M. J. *Langmuir* **2004**, *20*, 4101.
(41) Yang, D.; Krasowska, M; Sedev, R.; Ralston, J. *Phys. Chem. Chem. Phys.* **2010**, *12*, 13724.
(42) Franks, G. V.; Meagher, L. *Colloids Surf., A* **2003**, *214*, 99.

Table 4. CO_2-TPD Data for Alkaline Sites for Undoped and Selected Doped α-Al_2O_3 Nanosheets

sample	S_{BET} ($m^2\ g^{-1}$)[a]	T_{max} (°C)[b]	V_{CO2} (cm^3STP g^{-1})[c]	n_{CO2} (μmol g^{-1})[d]	CAS ($CO_2\ nm^{-2}$)[e]
ANS	19.1	668	6.67	298	9.4
Li-ANS	19.7	626	4.45	199	6.1
Mg-ANS	15.7	676	7.13	318	12.2
Ca-ANS	23.6	662	4.74	212	5.4

[a] Specific surface area calculated in the relative pressure range of 0.05−0.20 using the BET equation. [b] Temperature of maximum rate of desorption. [c] Standard total volume of carbon dioxide desorbed. [d] Amount of basic sites calculated by integration of the TPD profiles. [e] Surface concentration of active sites obtained from the amount of basic sites per unit area of the sample.

Applications of the α-Al_2O_3 Nanosheets. The doped and undoped α-Al_2O_3 nanosheets could find multiple applications in the chemical industry (catalysis) and materials processing (chemical-mechanical planarization, composites, ceramics) and are currently being tested in a variety of applications. Among the catalytic reactions that could benefit from using doped α-Al_2O_3 nanosheets are the following: ethylene oxide (EO) and propylene oxide (PO) catalyst carriers, CO oxidation catalysts, oxidation of organic vapors emissions in various chemical processes, deep oxidation of automotive emissions, hydration of EO to ethylene glycol (EG), diesel exhaust oxidation, and many other uses in catalysis where the α-Al_2O_3 nanosheets may offer advantages over traditional alumina-based supports. In chemical-mechanical planarization (CMP) applications, the nanosheets after deagglomeration have a great potential to act as thin and hard platelets to help in obtaining very smooth surface finishes. Presence of silica on the surface and the surface charge control enables wider range of slurry variations than for standard alumina particles. Composites containing the α-Al_2O_3 nanosheets or porous frameworks of these nanosheets could include ceramic−polymer, ceramic−metal, and ceramic−ceramic structures for a variety of refractory, structural, or chemical applications. In fact, as-synthesized α-Al_2O_3 nanosheets without any postsynthesis treatments form porous ceramic bodies with porosity of about 90% and good mechanical strength.[17] A successful fabrication of composites consisting of mesoporous carbon with enlarged pores being perpendicularly oriented to the c-facets of the α-Al_2O_3 nanosheets was recently reported.[43] Presence of dopants enables better microstructural control during sintering of the α-Al_2O_3 nanosheets in order to prepare porous or dense α-Al_2O_3 ceramics. For example, fabrication of zirconia-toughened alumina (ZTA) ceramics may be possible using Zr-ANS as starting materials.

(43) Górka, J.; Jaroniec, M.; Suchanek, W. L. *Nanoscale* **2010**, *2*, 2868.

Conclusions

The low-temperature hydrothermal method was used to synthesize novel types of α-Al_2O_3 nanosheets with controlled chemical compositions that can be applied in catalysis, composites, and other important applications. In this work, metals from nearly every group of the Periodic Table were examined as potential dopants of the α-Al_2O_3 nanosheets. It is shown that this doping resulted in a dramatic modification of the surface properties of alumina nanosheets without affecting the bulk of the material. The unprecedented thermal stability of these materials up to 1200 °C makes them even more attractive in applications, where other α-Al_2O_3 nanomaterials exhibit significant surface area loss, such as heterogeneous catalysis.

Acknowledgment. Financial support was provided by Sawyer Technical Materials, LLC. The authors are grateful to Mark Polster and Scott Klimek (both Sawyer Technical Materials, LLC, Eastlake, OH) for discussions and constant interest in the present work; Paul Lawson (Sawyer) for managing the autoclave operations; David Sherrick (Sawyer) for technical assistance; Dr. Wayne Jennings (Case Western Reserve University, Cleveland, OH) for XPS assistance; Dr. Reza Sharghi (Case) for TEM analysis; Dr. Łukasz Zych, Mr. Radosław Lach, and Dr. Mirosław M. Bućko (all AGH-University of Science and Technology, Kraków, Poland) for zeta potential measurements; Dr. Manik Mandal and Prof. Michał Kruk (both College of Staten Island, CUNY, New York, NY) for SAXS measurements.

Supporting Information Available: One figure with SAXS pattern, one figure with CO_2-TPD plots, and four figures showing HRTEM-STEM-XEDS analysis of the undoped and selected alkali metal doped α-Al_2O_3 nanosheets (PDF). This material is available free of charge via the Internet at http://pubs.acs.org.